

The nonlinear evolution of rotating configurations of uniform vorticity

By DAVID G. DRITSCHEL †

Geophysical Fluid Dynamics Program, Princeton University, Princeton, NJ 08540, USA

(Received 25 March 1985 and in revised form 24 January 1986)

The nonlinear evolution of perturbed equilibrium configurations of constant-vorticity vortices is calculated. To illustrate a variety of nonlinear behaviour, we consider the following relatively simple configurations: the corotating configurations of N vortices whose linear stability has been treated in a previous study; the elliptical vortex; and the annular vortex. Our calculations test for *nonlinear* stability as well as categorize the possible forms of stability and instability. The energy ideas announced in the previous study are found to greatly constrain vortex evolution. In particular, we show that two vortices and an elliptical vortex may evolve into each other, and that an annular vortex may break cleanly into five co-rotating vortices.

1. Introduction

We investigate the two-dimensional, nonlinear evolution of *piecewise-constant* vorticity distributions in an inviscid, incompressible and unbounded fluid. Particular interest is paid to initial conditions that are close to certain corotating equilibria, in an attempt to extend linear and nonlinear stability results and to categorize the full spectrum of evolutionary behaviour for certain simple configurations: elliptical, annular and multiple vortices (Dritschel 1985). We find that these configurations, when disturbed, in some instances evolve ‘close’ to other equilibria. How close depends crucially upon energy and angular momentum similarities between the equilibria and to a lesser extent upon the precise initial perturbation. First, however, we review many of the ideas that underpin the present study.

Originally, Deem & Zabusky (1978*a, b*) began exploring the evolution of certain piecewise-constant vorticity distributions after having discovered that the dynamics of these distributions depend only upon the boundaries or contours that separate uniform regions of vorticity. Zabusky, Hughes & Roberts (1979) presented further simulations of what they termed ‘contour dynamics’. Zabusky (1981), Overman & Zabusky (1982), Wu, Overman & Zabusky (1984), and others have continued research on the dynamics of interacting vortices. These works have dealt with improving the numerical algorithm, performing calculations with more complex initial conditions (some of which are repeated here), finding new equilibria, and numerically testing the stability of equilibria.

Before the advent of contour dynamics, the only known equilibria were in the form of circular distributions of vorticity and ellipses (Kirchoff 1876). More than a century passed before new equilibria were found, and computational methods were then necessary. Deem & Zabusky (1978*a, b*) found several members of certain families of equilibria: m -fold single-vortex states ($m = 2$ corresponds to the family of ellipses) and translating two-vortex states. Subsequently, solutions were calculated by

† Present affiliation: Department of Applied Mathematics and Theoretical Physics, University of Cambridge, Cambridge CB3 9EW, UK.

Saffman & Szeto (1980) for a pair of equal, corotating vortices, Pierrehumbert (1980) for the entire family of translating two-vortex states, Pierrehumbert & Widnall (1981) for a linear array of identical vortices, Zabusky (1981) for two unequal (translating and rotating) vortices, Saffman & Schatzman (1982) for a vortex street (two rows of oppositely signed identical vortices), and Dritschel (1985) for 2–8 corotating vortices.

In parallel with the search for new equilibria came the examination of stability. Linear stability calculations have been performed *analytically* for the ellipse by Love (1893) and for the annular vortex by Michalke & Timme (1967) (see also Snow 1978 and Childress 1984). More complicated equilibria have required numerical solutions of the eigenvalue problem; Saffman & Schatzman (1982) and later Meiron, Saffman & Schatzman (1984) determined the stability of vortex streets for a subset of possible equilibria, while Dritschel (1985) found the stability of 2–8 corotating vortices. Stability has also been tested by calculation. Some instabilities associated with elliptical vortices are presented by Zabusky (1981), and Overman & Zabusky (1982) show two corotating vortices ‘merging’ or sliding very close to each other. In the past three years, several analytical nonlinear stability theorems have been proven. Nonlinear stability guarantees that a sufficiently small (but finite) disturbance will never grow larger than a fixed size (as measured in a certain norm defined below). Wan & Pulvirenti (1985) have proven that the circle is stable. Tang (1984) has shown that the ellipse is non-linearly stable in the same range of aspect ratios that imply linear stability – an interesting result because although stability automatically implies linear stability, the reverse is not always true. Marsden (1985) presents an excellent review of the recent developments in stability theory.

From a mathematical standpoint, uniform-vortex evolution represents an infinite-dimensional dynamical system with stability properties at most poorly understood (Dritschel 1985). Calculations of linear stability are formidable computational problems, yet linear stability does not guarantee stability in general. An imposed disturbance, taking the form of a finite-amplitude eigenmode of the linear stability analysis, may lead to instability even though linear theory predicts stability. Either the initial disturbance excites unstable eigenmodes through nonlinear interactions, or the disturbance evolves outside the scope of linear theory, independent of the disturbances’ amplitude. It is this latter possibility that has motivated recent mathematical interest in the nonlinear stability of uniform vortices. The existing proofs of (nonlinear) stability bound the disturbance with respect to area but not arc length; specifically the amount of circulation that may cross an iso-vorticity contour is bounded for all time (the L_1 norm) – see Marsden (1985). A ‘stable’ disturbance may nonetheless form long wisps of small area, a process not describable by linear theory. For more complex equilibria, analytical proofs of stability do not yet exist, and the already intricate proofs for the circle and the ellipse point to the need for direct numerical calculation.

The purpose of this paper is to more clearly ascertain the range of behaviours associated with evolving vortex configurations of initial states close to rotating equilibria. Many calculations of vortex evolution have appeared in the literature, and we do not intend to simply add to the list – instead, several particular configurations are examined thoroughly in order to understand their nonlinear morphologies. Our task is threefold. (i) We discuss the relationship, if any, between linear stability and the evolution of finitely perturbed equilibria. The analytical nonlinear stability results suggest that finite disturbances can evolve in a way not predicted by linear theory (e.g. by ejecting thin strands of vorticity). Also, nonlinear wave–wave interactions

can generate linearly unstable disturbances which may then grow according to linear theory, at least initially. (ii) We show how the correspondence of certain globally conserved quantities (such as circulation, angular momentum and energy) can explain the transition of one near-equilibrium to another of radically different character, and (iii) how the *lack* of correspondence between one equilibrium's conserved properties and those of all other equilibria lead to 'cascading' or the generation of much fine-scale vorticity structure.

This study of nonlinear stability germinated in a recent study of the linear stability of configurations of corotating vortices, Dritschel (1985, hereinafter referred to as D), and, because the current study depends crucially upon that work, the reader should refer to it for background material; many of the details regarding the family of corotating vortices – their shapes, linear stability and energetics – may be found in that work and will not be reiterated here. The current study extends the linear stability analysis of D to finite-amplitude perturbations and confirms the utility of energetics in understanding nonlinear evolution. A brief review of energetics appears in the next section. In §3 we describe a contour-dynamics numerical algorithm which is then used to investigate the nonlinear morphology of certain equilibrium configurations: an annular region of vorticity (§4), an elliptical vortex (§5), and the corotating configurations discussed in D (§6). These particular configurations are studied because of their simplicity, their nonlinear evolutionary relationships, and their relevance to geophysical phenomenon (§7).

2. Energetic constraints on nonlinear evolution

Energy and angular-momentum conservation strongly constrain the evolution of vortex configurations. Indeed, the proofs of nonlinear stability for the circle and the ellipse (Wan & Pulvirenti 1985; Tang 1984) follow directly from these conservation relations. It is therefore expected that an examination of the energetic constraints will yield important additional information about vortex evolution not already contained in the linear disturbance framework. In this way, energy bridges linear and nonlinear stability. We derived some constraints in D applicable to arbitrary distributions of vorticity, $\omega(x, y)$. By restricting the analysis to piecewise-constant distributions in an inviscid fluid, the conserved quantities, now only finite in number, take on especially simple forms:

the area of each vortex	$A_j, j = 1, 2, \dots, N,$	}	(2.1)
the vorticity of each vortex	$\omega_j,$		
the total circulation	$\Gamma = \iint \omega \, dx \, dy = \sum_j \omega_j A_j,$		
the angular momentum	$J = 2 \iint (x^2 + y^2) \omega \, dx \, dy,$		
the centroid	$\bar{x} = \iint \frac{\omega x \, dx \, dy}{\Gamma}, \quad \bar{y} = \iint \frac{\omega y \, dx \, dy}{\Gamma},$		
the 'excess' energy	$T_s = \lim_{L \rightarrow \infty} \left\{ \frac{1}{2} \iint (u^2 + v^2) \, dx \, dy - \frac{\Gamma^2}{4\pi} \log \left(\frac{L}{l} \right) \right\},$		

where the lengthscale $l \equiv (J/\Gamma)^{\frac{1}{2}}$ and L is the radius of the outer 'boundary' of the flow, as we take this radius to infinity. The definition of T_s is necessary because the actual energy of an unbounded fluid with circulation is infinite. Γ is listed for

convenience even though it depends on some of the other conserved quantities. (See the Appendix for Γ , J and T_s in terms of contour integrals.)

For vorticity distributions with non-zero circulation, the two fundamental conserved quantities are the angular momentum and the energy. We can always transform coordinates so that $\bar{x} = \bar{y} = 0$ whereas the ω_j are trivially conserved. In D, the ω_j and the A_j were used to cast the energy and angular momentum into non-dimensional terms, E and A^{-1} below. Define

$$\left. \begin{aligned} \text{the energy } E &= \frac{16\pi T_s}{\Gamma^2}, \\ \text{and the inverse angular momentum } A &= \frac{\Gamma^3}{\pi J \eta}, \end{aligned} \right\} \quad (2.2)$$

where $\eta = \iint \omega^2 dx dy = \sum_j \omega_j^2 A_j$ is the total enstrophy. For a circular vortex, $E = A = 1$. In the present study, the vorticity distributions are not only piecewise constant but also have the same uniform value of the vorticity. In such a case A represents the total dimensionless area of the rotational fluid: $A = \sum_j A_j / \pi l^2$ and $0 \leq A \leq 1$. Such vorticity distributions have the convenient property that E and A are directly related. Figure 1 shows $E(A)$ for the known rotating equilibria. In D we used the energy curves of *different* vortex configurations to make predictions about possible transitions between configurations. We show later that figure 1 is fundamental to understanding such transitions, and we exemplify this by the breakup of an annulus into five corotating vortices (§4), the breakup of an ellipse into two vortices (§5), and the merger of two vortices into an ellipse (§6).

3. The contour-dynamics algorithm

When a two-dimensional, inviscid, incompressible, boundless fluid is assumed to consist of regions of constant vorticity, the velocity at any point is known solely in terms of the positions of the boundaries of vorticity discontinuity. Specifically, the velocity depends on contour integrals around each of the different regions of vorticity (vortices). The standard procedure has been to discretize the vortex boundaries (see Wu *et al.* 1984 and the references therein). Our approach has been basically the same with a slight modification in performing the contour integrals. Between every two (nodal) points X_i and X_{i+1} on a given vortex boundary, we interpolate with a *local* cubic in a coordinate system whose x -axis runs parallel to the vector between nodes i and $i+1$. Let $t = X_{i+1} - X_i$ and $n = \hat{z} \wedge t$ be the local tangent and normal vectors respectively. Then, for $X_i \leq X \leq X_{i+1}$, $X(p) = X_i + pt + \eta(p)n$, where η is assumed to be the cubic $\alpha p + \beta p^2 + \gamma p^3$ for $0 \leq p \leq 1$. α , β , and γ are determined by forcing the cubic to pass through the four points X_{i-1} , X_i , X_{i+1} and X_{i+2} (the condition at X_i has already been imposed).

A more accurate method was employed to calculate the velocity field contour integral, which avoids direct use of the logarithmic Green's function. Referring to equation (2.7) of D, the key is to notice that the velocity field at a point due to vortex boundaries located at X_k ($k = 1, \dots, N$), i.e.

$$u(x) = -\frac{1}{4\pi} \sum_{k=1}^N \omega_k \oint_{C_k} \log|x - X_k|^2 dX_k, \quad (3.1)$$

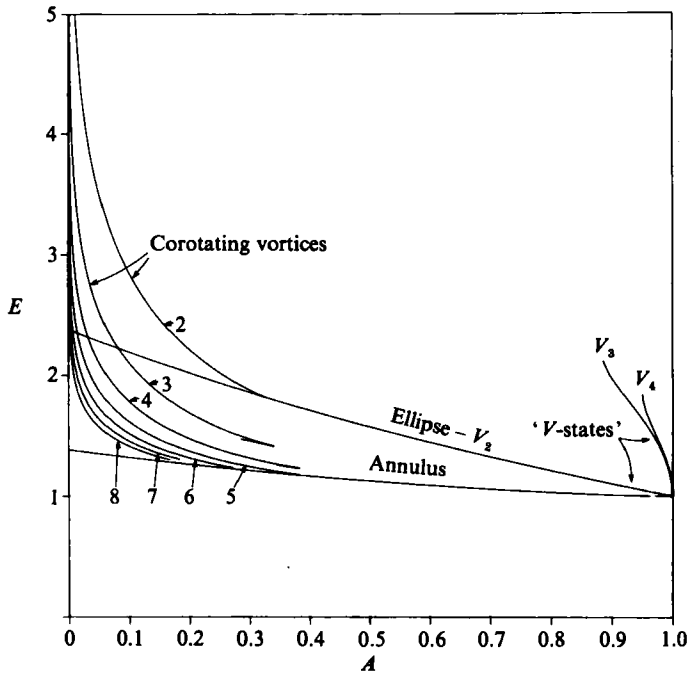


FIGURE 1. The energy-area diagram for the rotating equilibria of a single uniform vorticity. The corotating vortices, elliptical vortices, annular vortices, and the N -fold symmetric single vortex states, V_N (see Wu, Overman & Zabusky 1984) are shown.

can be transformed via an integration by parts to

$$u(\mathbf{x}) = \frac{1}{2\pi} \sum_{k=1}^N \omega_k \oint_{C_k} (\cos \theta, \sin \theta) (\cos \theta dX_k + \sin \theta dY_k), \quad (3.2)$$

where $(\cos \theta, \sin \theta) = (\mathbf{x} - \mathbf{X}_k) / |\mathbf{x} - \mathbf{X}_k|$. The numerical advantage is that the integrand of (3.2) is non-singular if \mathbf{X}_k passes through \mathbf{x} whereas that of (3.1) is singular.

Next, the velocity at a given nodal point is calculated from contour integrals performed using four-point Gaussian quadrature (Abramowitz & Stegun 1965, p. 921) between each pair of nodes along the entire boundary of each vortex. Once this is done for each nodal point, the system is integrated in time by means of either a fourth-order Runge-Kutta or a 'leap-frog' scheme. We do *not* adjust the nodal positions for purposes of resolution after the points are laid down at the initial time. Such an adjustment scheme could have been useful in several instances, but would not have allowed us to continue the calculations much longer than we did (see below).

All calculations were performed on a Cyber 205 vector processing supercomputer. Test calculations were performed to assess the optimal timestep, quadrature formula, and spatial resolution, and the results proved insensitive to further adjustments of parameters except when regions of high curvature developed or when contour perimeters grew unreasonably long. The algorithm was also checked against known results such as the rotation rates of ellipses and multiple vortices as well as phase speeds of waves on a circular vortex. During the calculations, circulation and angular momentum were used as diagnostics to measure accuracy, and significant departures from conservation of these quantities were found to correspond to severe contour deformations.

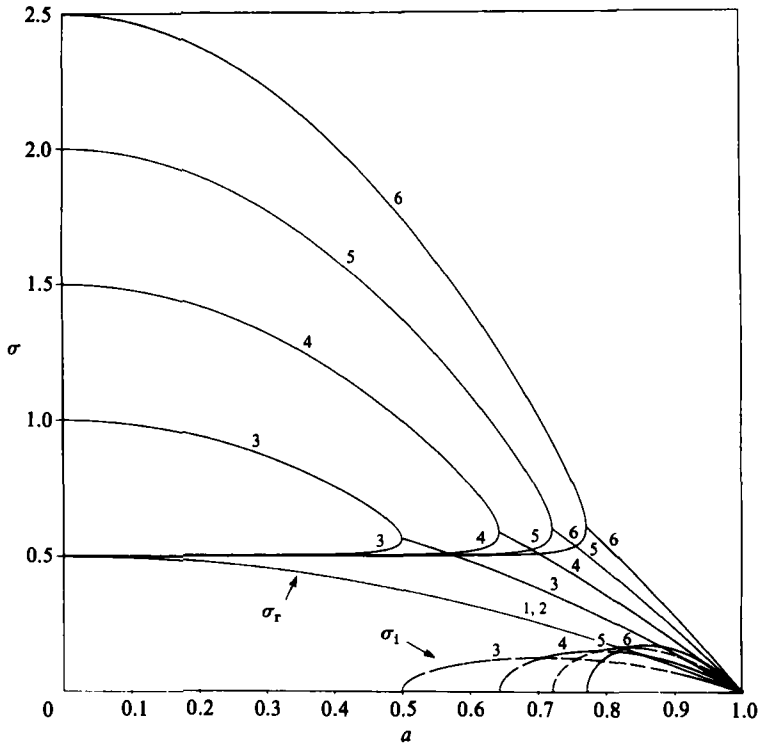


FIGURE 2. The stability of an annular vortex of unit vorticity. At $a = 0$, there are two real frequencies (solid lines), $\sigma = \frac{1}{2}(m-1)$ and $\sigma = \frac{1}{2}$: the first corresponds to the solid circular vortex while the second is due to the hole at the vortex centre. The two frequencies join up causing instability (dashed lines) until $a = 1$.

4. Annular-vortex evolution

In this section, we examine the behaviour of small perturbations to an annular region of vorticity. We begin by reviewing the linear stability of an annular vortex. Finite-amplitude eigenmodes from the linear stability analysis are then added to this annulus, and the system is integrated in time for a variety of basic-states and disturbances. Also, the effect of more general disturbances is discussed.

The linear stability of the annular vortex was first determined by Michalke & Timme (1967). For continuity, we shall present the principal results. The annular vortex is defined to be a ring of unit vorticity lying radially between a and 1. The eigenfunctions are sinusoidal boundary waves of the form $\text{Re}[\exp(im(\theta - \beta_2) - i\sigma t)]$ on the outer boundary and $a^{m-1} \text{Re}[1/(1+2\sigma) \exp(im(\theta - \beta_1) - i\sigma t)]$ on the inner boundary with $0 \leq \theta \leq 2\pi$. Here, m is the azimuthal wavenumber while the phase difference $\Delta\beta \equiv \beta_2 - \beta_1 = \tan^{-1}[\text{Im}(2\sigma)/\text{Re}(1+2\sigma)]$. The eigenvalue σ is given by

$$\sigma(m, a) = \frac{1}{4}m(1-a^2) \pm \frac{1}{2}[(1 - \frac{1}{2}m(1-a^2))^2 - a^{2m}]^{\frac{1}{2}}. \quad (4.1)$$

Figure 2 shows σ versus a for $m = 1$ to 6. The vortex is unstable if $a > \frac{1}{2}$ with the first instability being 3-fold symmetric. A 4-fold instability is possible for yet thinner annuli, $a > (\sqrt{2}-1)^{\frac{1}{2}}$, and higher values of m become unstable as a approaches unity,

Two series of calculations are described. Each calculation begins with 100 uniformly distributed nodes on each boundary. Time is measured relative to the quantity $T = 4\pi J/\Gamma^2 = (1+a^2)/(1-a^2)$. In the first series of calculations, the initial

a	m	Basic-state type	Disturbance type	Nonlinear stability
0.2, 0.4	3, 4, 5	Stable	Neutral	Stable
0.5	2, 4	Marginal	Neutral	Stable
0.5	3 ³	Marginal	Marginal	Unstable
0.6	2, 4 ⁴ , 5, 6	Unstable	Neutral	Stable
0.6	3	Unstable	Stable, unstable	Unstable
0.7	5, 6	Unstable	Neutral	Stable
0.7	3, 4	Unstable	Stable, unstable	Unstable
0.7	2 ⁶	Unstable	Neutral	Unstable

TABLE 1. A summary of the calculations performed in series 1. For neutral disturbances, both values of σ in (4.1) were considered. All calculations were done using perturbation amplitudes ϵ of 0.01, 0.02 and 0.05. Superscripts denote figure numbers

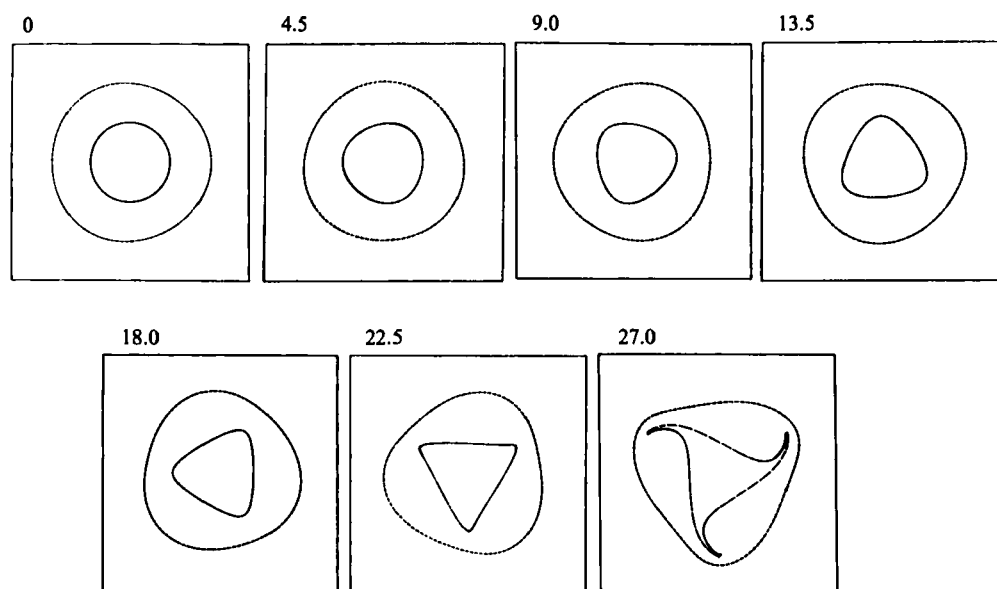


FIGURE 3. Breakup into multiple vortices of a marginally stable vortex ($a = 0.5$) due to a superimposed marginal disturbance ($m = 3$). $\epsilon = 0.02$.

condition consists of an annulus (defined by the parameter a) plus an eigenmode from the linear stability analysis (defined by m) multiplied by a small number ϵ . We consider three basic states: (i) total linear stability ($a < \frac{1}{2}$); (ii) marginal stability ($a = \frac{1}{2}$); and (iii) linear instability ($a > \frac{1}{2}$). Furthermore, we consider four disturbance types that apply to each m individually: (i) neutral (the m -fold disturbance is neutral, $\text{Im}(\sigma) = 0$), (ii) marginal (for $m = 3$, a must be $\frac{1}{2}$ while for $m = 4$, a must be $(\sqrt{2} - 1)^{\frac{1}{2}}$); (iii) unstable ($\text{Im}(\sigma) > 0$) and (iv) stable ($\text{Im}(\sigma) < 0$).

The three basic states were tested for stability by imposing various kinds of disturbances with amplitudes ϵ of 0.01, 0.02 and 0.05 (see table 1). When the basic state is linearly stable, only neutral disturbances are possible, and these are always (nonlinearly) stable (in the area norm, not arc length). But, for a marginal basic state ($a = \frac{1}{2}$), a marginal disturbance ($m = 3$) does lead to instability (figure 3). Thus the instabilities associated with annular vortices do cause the ring of vorticity to ‘break’

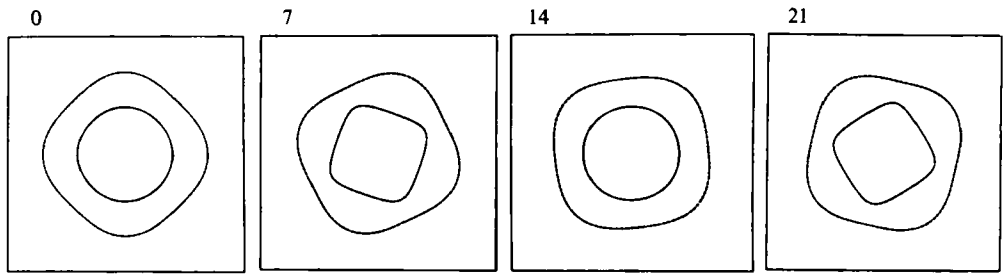


FIGURE 4. Nonlinear vacillation of a neutral mode ($m = 4$) on a linearly unstable vortex ($a = 0.6$). The amplitude of the initial disturbance is $\epsilon = 0.05$.

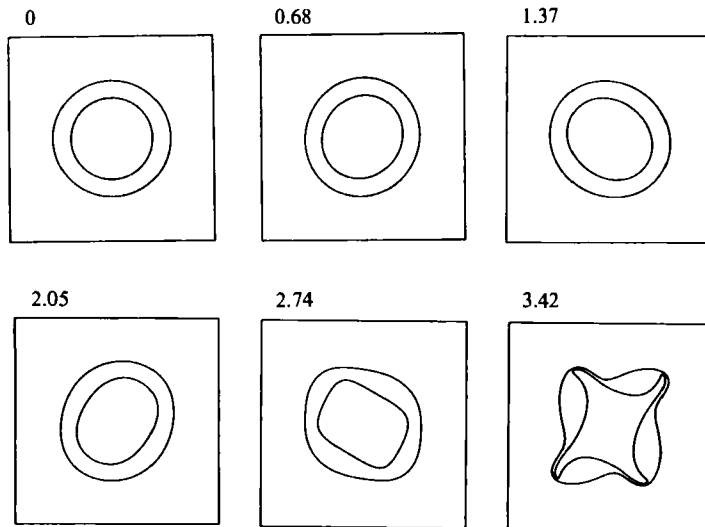


FIGURE 5. Instability of a neutral $m = 2$ disturbance on an unstable basic state. $a = 0.7$ and $\epsilon = 0.01$.

into multiple vortices – the ring does not actually break because the fluid is inviscid. In any case, it is clear that several distinct centres of vorticity develop. If the basic state is unstable ($a > \frac{1}{2}$), but the imposed disturbance is neutral, as when $a = 0.6$ and $m = 4$ (figure 4), the initial condition regularly repeats itself except for a phase shift. We term this *near-recurrent* motion vacillation, and this behaviour is found to be typical for neutral disturbances to an unstable vortex, with one exception. When the vortex is sufficiently thin to excite 4-fold linear instabilities, 2-fold disturbances lead to instability via wave-wave interactions (figure 5). The reverse is not true. For instance, a neutral 6-fold disturbance cannot destabilize a vortex that is at most linearly unstable to $m = 3, 4$ and 5 – higher- m disturbances cannot destabilize lower- m disturbances. Finally, we found that all linearly *stable* disturbances nevertheless lead to the breakup of the annulus. Apparently, a stable disturbance (with eigenvalue σ , say) excites its unstable conjugate (with eigenvalue σ^* , where $*$ denotes complex-conjugation).

In a second series of calculations (see table 2), we simply added $0.1 \cos m(\theta - \beta_j)$ to each boundary of the annulus and considered several phase differences. Because this is *not* an eigenmode from the linear stability analysis, many eigenmodes are

a	m_2	m_1	$m_1\beta$	Basic-state type	Nonlinear evolution
0.4	5	5	0 ⁶ , 90, 180	Stable	Steep, sharp waves
0.4	5	4	0	Stable	Steep, sharp waves
0.4	4	5	0	Stable	Steep, sharp waves
0.5	3	3	0, 90, 180	Marginal	Three vortex centres
0.5	2	2	0, 90	Marginal	Vacillation
0.5	4	4	0, 45	Marginal	Vacillation
0.6	3	3	0, 90, 180	Unstable	Three vortex centres
0.6	2	3	0	Unstable	Complex instability
0.6	3	2	0	Unstable	Complex instability
0.6	3	4	0	Unstable	Complex instability
0.6	4	3	0	Unstable	Complex instability
0.6	4	4	0, 45	Unstable	Vacillation
0.6	5	5	0, 180	Unstable	Vacillation
0.7	1	1	0	Unstable	Complex instability
0.7	1	2	0, 90 ⁷	Unstable	Complex instability
0.7	2	1	0, 90	Unstable	Complex instability
0.7	2	2	0, 90 ⁸	Unstable	Complex instability
0.7	2	3	0	Unstable	Complex instability
0.7	3	2	0	Unstable	Complex instability
0.7	2	4	0	Unstable	4 Unequal vortices
0.7	4	2	0	Unstable	4 Unequal vortices
0.7	4	4	0, 45 ⁹	Unstable	4 Vortices
0.7	4	5	0	Unstable	Complex instability
0.7	5	4	0	Unstable	Complex instability
0.7	5	5	0, 180 ¹⁰	Unstable	5 Vortices

TABLE 2. A summary of the calculations performed in series 2. The inner boundary disturbance is $0.1 \cos m_1(\theta - \beta)$ and that of the outer boundary is $0.1 \cos m_2\theta$. Superscripts denote figure numbers

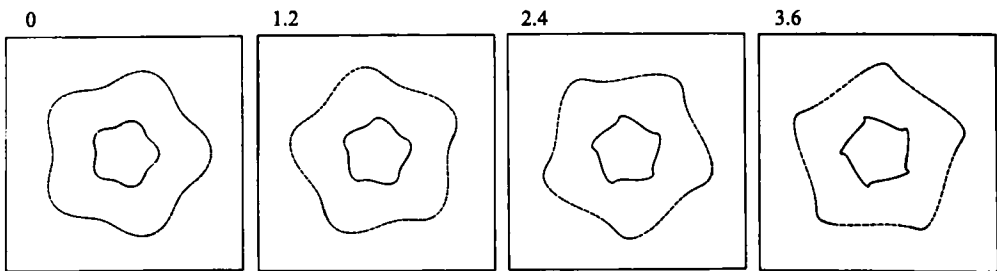


FIGURE 6. Nonlinear stability in the form of steep, small waves. $a = 0.4$, $m = 5$, and $\epsilon = 0.1$.

present. A second form of nonlinear *stability* (other than vacillation), which appears to be restricted to linearly stable basic states, is demonstrated in figure 6 ($a = 0.4$, $m = 5$). The boundary waves become steep and sharp but never carry away a significant amount of the circulation. In other words, the area of the perturbation is bounded by an amount related to the initial perturbation area, which is in fact the definition of stability used by Wan & Pulvirenti (1983) and others to prove nonlinear stability analytically. Deem & Zabusky (1978*a, b*) first observed sharpening (and desharpening) waves near the ‘corners’ of a singly connected 3-fold symmetric vortex state, see also figure 7 of Zabusky (1981). Vacillation occurs only if the disturbance is free from an $m = 3$ component *and* even disturbances are linearly stable

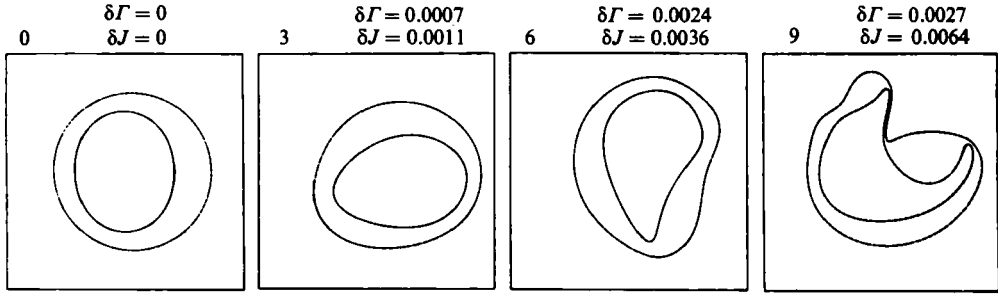


FIGURE 7. 2-1 disturbance breakup of an unstable vortex. $a = 0.7$ and $\epsilon = 0.1$. $\delta\Gamma$ and δL track the fractional changes in circulation and angular momentum with time.

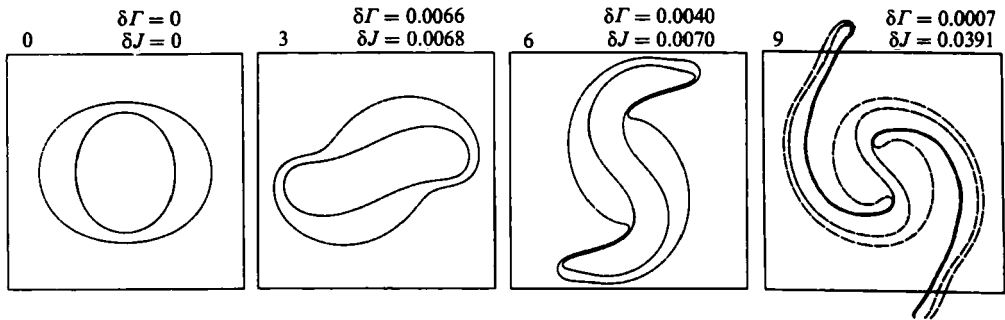
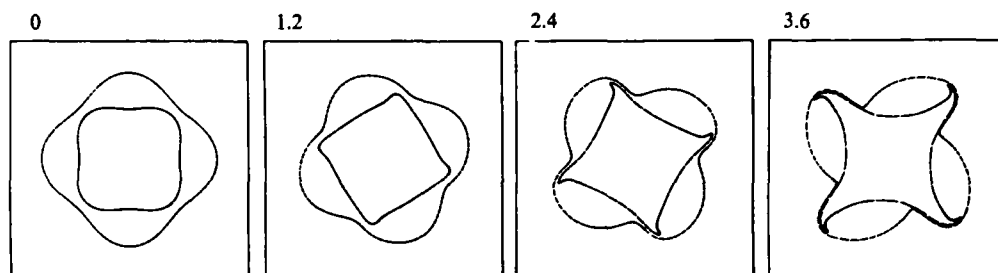
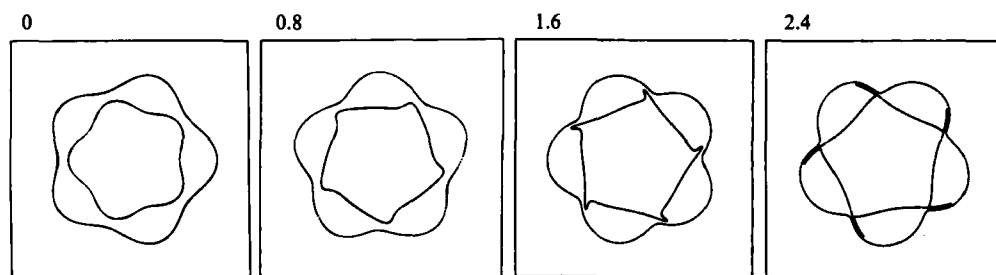


FIGURE 8. 2-2 disturbance breakup and subsequent merger of an unstable vortex. $a = 0.7$ and $\epsilon = 0.1$.

($a < (\sqrt{2}-1)^{\frac{1}{2}}$). Other combinations of basic states and disturbances lead to major alternations of the initial configuration.

Figure 7 starts with an $m = 2$ disturbance on the inner boundary and an $m = 1$ disturbance on the outer boundary – for reference we call this a 2-1 disturbance. In this figure, we track the relative change in circulation, $\delta\Gamma$, and angular momentum, δJ , as a measure of accuracy. These quantities change by less than 1% during the calculation. As a result of the symmetry differences between the inner- and outer-boundary disturbances, the evolution is totally void of symmetry. In contrast (figure 8), a 2-2 disturbance evolves into two elongated vortices which spiral toward the origin. Owing to the generation of long strips of vorticity, the resolution rapidly deteriorates. But, a 2-4 disturbance evolves into four unequal-sized (but partly symmetric) vortices with little ejection of vorticity into the fluid surrounding the vortices (not shown). Two additional examples that evolve relatively cleanly are shown in figures 9 and 10. In figure 9 four skewed vortices develop (see also the point-vortex cloud calculation of Christiansen 1973) but the five vortices in figure 10 are nearly symmetric, and, in fact look much like the limiting member of the equilibrium family of five vortices (figure 2*d* of D). This can be understood by considering figure 1: a transition is almost possible between the limiting member of the family of five corotating vortices and an $a = 0.7$ annular vortex (at $A = 0.38$). For fewer than five vortices, clean transitions between annuli and *symmetric* corotating vortices are not possible because of their energetic dissimilarities. The results of figure 10 underscore the utility of energetics in understanding transitions.


 FIGURE 9. 4-4 disturbance. $a = 0.7$ and $\epsilon = 0.1$.

 FIGURE 10. 5-5 neutral disturbance superimposed on an unstable vortex, $a = 0.7$. The amplitude is large enough ($\epsilon = 0.1$) to form multiple vortices.

We have determined that a linearly stable ($a < \frac{1}{2}$) annular vortex is stable to sufficiently small disturbances. If the basic state is linearly unstable to both even and odd disturbances, only neutral eigenmodes with $m \neq 2$ are stable; $m = 2$ can generate the $m = 4$ unstable eigenmode (figure 4). For thicker annuli in which only $m = 3$ is unstable, it takes a disturbance with a 3-fold component to cause instability. Linearly marginal, unstable *and* stable disturbances always lead to instability. The stable modes nonlinearly generate their unstable counterparts. As for the character of the evolution, nonlinearly stable disturbances either vacillate or form sharp, steep boundary waves, whereas unstable disturbances tend to break apart the ring of vorticity.

5. Elliptical-vortex evolution

Love (1893) determined analytically the linear stability of the ellipse. He discovered that instability may occur if the major-to-minor axis length ratio exceeds 3 to 1. We first present a review of Love's main results and then examine the nonlinear behaviour of slightly perturbed ellipses†. We intend to relate nonlinear stability to linear stability, but, additionally, we shall discuss the interesting connection between ellipses and two corotating vortices whose energy curves intersect twice. This leads us to propose a direct relationship between energetics and nonlinear evolution.

The elliptical vortex is defined as a vortex with semi-minor axis b , semi-major axis a , and unit vorticity. Its boundary shape is given parametrically by $x_0 = a \cos \theta$ and

† Zabusky (1981) also presents a number of relevant calculations.

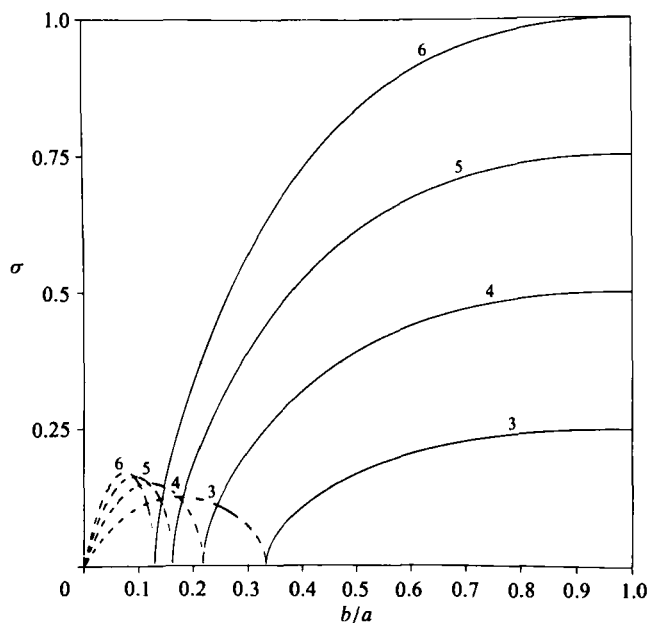


FIGURE 11. The stability of an elliptical vortex of unit vorticity after Love (1893). Stability of a given azimuthal mode occurs from $b/a = 1$ until the wave frequency (solid lines) goes to zero. Then, the frequency remains zero while the growth rate (dashed lines) becomes non-zero until $b/a = 0$.

$y_0 = b \sin \theta$, $0 \leq \theta \leq 2\pi$. For a given 'azimuthal' wavenumber m the eigenfunction has the structure

$$(\Delta x, \Delta y) = \frac{\epsilon(-b \cos \theta, a \sin \theta) \cos m(\theta - \beta)}{b^2 \cos^2 \theta + a^2 \sin^2 \theta}. \quad (5.1)$$

The phase β is zero as long as the eigenvalue, $\sigma = \pm (EF)^{\frac{1}{2}}$, is real; here $E = m\Omega - \frac{1}{2}(1 + \gamma)$, $F = m\Omega - \frac{1}{2}(1 - \gamma)$, $\gamma = [(a - b)/(a + b)]^m$, and $\Omega = ab/(a + b)^2$ is the rotation rate of the unperturbed ellipse. Otherwise, $\tan m\beta = \pm (-E/F)^{\frac{1}{2}}$ for the unstable and stable modes respectively. Figure 11 shows positive $\sigma(b/a; m)$ for $m = 3$ to 6 (we do not show σ for $m = 1$ or 2 because $\sigma = \pm \Omega$ and 0 respectively; also, $\beta = \pm \frac{1}{4}\pi$ when $m = 2$). As $b/a \rightarrow 0$, some algebra shows that the wavenumber of maximum instability is given by $m = xa/b$ where $x \doteq 0.398406$ (the solution to $e^{-4x} - 2x + 1 = 0$) and the maximum growth rate is given by $\sigma = (\frac{1}{2}x - x^2)^{\frac{1}{2}} \doteq 0.201185$. This behaviour is already evident in figure 11 for relatively low values of m .

The nonlinear stability of the ellipse is considered next. Tang (1984) has recently proven analytically that the ellipse is stable whenever $\frac{1}{3} < b/a < 3$ (stable to disturbances whose amplitude goes to zero at the stability boundaries). Our numerical results are meant to confirm this result and to illustrate the range of behaviours associated with unstable ellipses. The following calculations begin with an ellipse plus eigenfunctions from the linear stability analysis. In each case, for a given perturbation symmetry m , we fix the phase $\beta = 0$. This is a single eigenfunction of the linear stability analysis whenever the basic state is linearly stable to m -fold disturbances. But, if the basic state is linearly unstable, the perturbation is the superposition of the stable and unstable eigenmodes. When $m = 2$, such a superposition is not possible because $\cos m(\theta - \beta) = \pm \sin 2\theta$ for $\beta = \pm \frac{1}{4}\pi$. To first order in disturbance amplitude, these eigenmodes preserve the elliptical shape by slightly tilting the vortex from its alignment in the (x, y) -plane (hence the zero eigenvalue). A perturbation with $\beta \neq \pm \frac{1}{4}\pi$ cannot be expressed in terms of the eigenmodes of the linear stability

b/a	m	Basic-state type	Disturbance type	Nonlinear stability
1, 1/2	2, 3, 4	Stable	Neutral	Stable
1/3	2, 4	Marginal	Neutral	Stable
1/3	3 ^{13a}	Marginal	Marginal	Unstable
1/4	2, 4	Unstable	Neutral	Stable
1/4	3	Unstable	Unstable	Unstable
1/4	5	Unstable	Neutral	Unstable
1/5	2	Unstable	Neutral	Stable
1/5	3, 4	Unstable	Unstable	Unstable
1/5	5, 6	Unstable	Neutral	Unstable
1/6	2 ^{12a}	Unstable	Neutral	Unstable
1/6	3 ^{12b} , 4 ^{12c}	Unstable	Unstable	Unstable
1/6	5 ^{12d} , 6, 7	Unstable	Neutral	Unstable
0.1655	2 ^{14a}	Unstable	Neutral	Unstable

TABLE 3. A summary of the elliptical vortex calculations. The disturbance is of the form of an eigenfunction with zero phase, except in the case when $m = 2$ (see text for discussion). The initial perturbation amplitude is $\epsilon = 0.01$. Superscripts denotes figure numbers

analysis because such a perturbation would violate the conservation of area, angular momentum and energy, quantities that are conserved to first order in disturbance amplitude by the linear eigenmodes. *Nevertheless*, we choose to perturb the ellipse with an $m = 2, \beta = 0$ disturbance as in (5.1). Finally, the amplitude $\epsilon = 0.01$ for all cases, and each calculation begins with 400 uniformly distributed (in θ) nodes.

We illustrate just a few calculations, but the complete list is given in table 3. Consider the evolution of a perturbed 6:1 ellipse ($b/a = \frac{1}{6}$). The basic state is linearly unstable to $m = 3$ and 4. In figure 12(a), a 2-fold symmetric disturbance rips the ellipse into two pieces, leaving a thin thread of vorticity connecting the two vortex centres. The two centres of vorticity so formed fall into the linearly stable regime of the analysis of D and, as is shown in the following section, linearly stable configurations are also nonlinearly stable. (Zabusky *et al.* 1979 indeed show two stable ‘pulsating’ vortices). Figure 12(b, c) shows the nonlinear instability of the linearly unstable $m = 3$ and $m = 4$ disturbances. In figure 12, the tail of vorticity that forms, if taken in isolation, would rapidly roll-up by the Kelvin–Helmholtz instability mechanism; however, the stretching effect on the tail by the central vortex counteracts this mechanism (see Saffman & Baker 1979 and Moore & Griffith-Jones 1974 for a discussion of the processes involved). Nevertheless, in this figure, the effect of the central vortex may not be sufficient to prevent an eventual catastrophic roll-up of the tail (see figure 8 of Zabusky 1981). In contrast, figure 12(c) shows a case ($m = 4$) in which the tails may be thinned rapidly enough to prevent eventual roll-up. Note the differences between figures 12(a) and (c); the $m = 2$ disturbance rips the vortex apart, whereas the $m = 4$ disturbance leaves the central vortex intact at the expense of ejecting thin streamers of vorticity. In figure 12(d), an ellipse perturbed with a linearly neutral 5-fold disturbance destabilizes by first ejecting a thin streamer of vorticity and then undergoing a broad, low-wavenumber distortion. 6- and 7-fold perturbations lead to similar evolutionary behaviour (not shown). We find that neutral disturbances with $m \neq 2$ excite the unstable eigenmodes through the distinctly nonlinear process of ejecting thin filaments, an irreversible process indicative of infinite-dimensional dynamical systems (water waves are another example – see Benjamin & Olver 1982).

When the basic-state ellipse is not too eccentric, so that it is linearly stable to

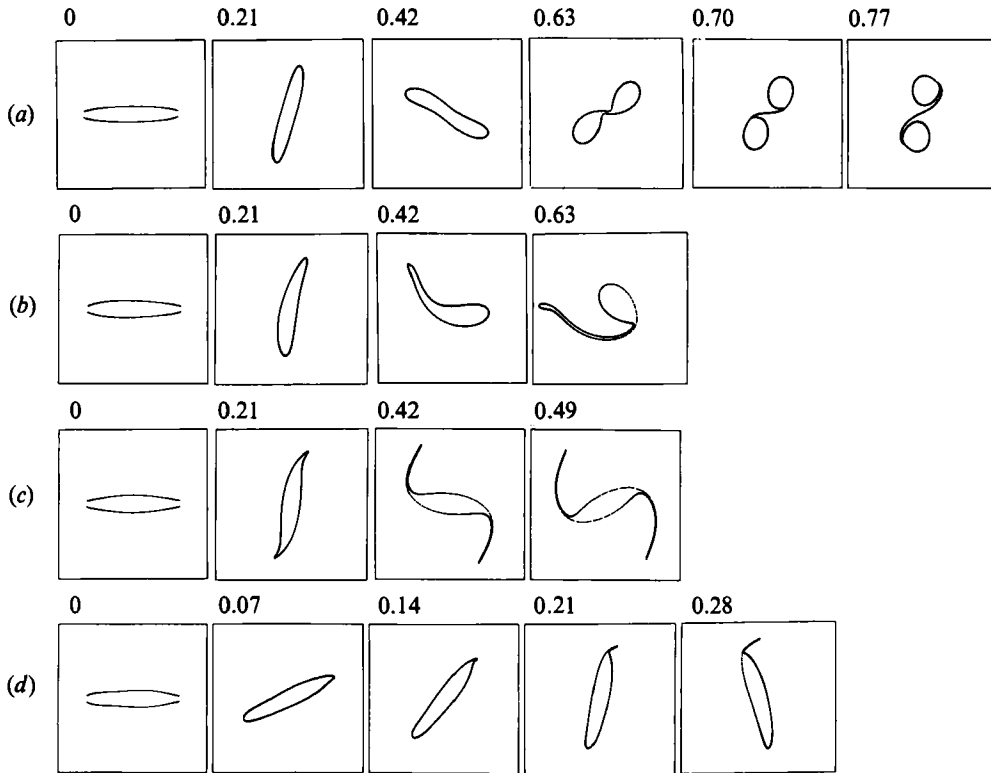


FIGURE 12. The stability of a 6:1 ellipse to various linear disturbances: (a) $m = 2$ (neutral), (b) $m = 3$ (unstable), (c) $m = 4$ (unstable), (d) $m = 5$ (neutral).

$m = 4$ disturbances, perturbations with even symmetry simply vacillate (see table 3). The even symmetry of the ellipse coupled with that of the disturbance can never generate the odd $m = 3$ linearly unstable eigenmode. When both $m = 3$ and 4 are linearly unstable, all disturbances (except as noted below) are nonlinearly unstable. Low- m disturbances ($m \leq 4$) create large-scale changes of the initial condition. High- m disturbances, however, first cause the ejection of thin streamers of vorticity before major structural alterations develop. 2-fold disturbances are only unstable at yet higher eccentricities.

The following example shows the accuracy and limitations of the numerical algorithm. The $m = 3$ marginal disturbance is nonlinearly unstable on a marginal ellipse (figure 13a). In contrast to the double 'tail' observed by Zabusky (1981) on a 3.5:1 ellipse, the 3:1 ellipse exhibits only a single tail. Figure 13(b) shows an enlarged version of the last frame of figure 13(a) in which the effects of poor resolution can be seen. Fig 13(c) is the same calculation but with 16 instead of a 4 Gaussian points between nodes, and while the numerical instability is not apparent, it reappears a few timesteps later. The instability is related to the inaccurate calculation of the velocity close to a contour.

We turn next to the relationship that exists between the elliptical vortex and two corotating vortices. In D, we found that there are two ellipses, $b/a = 0.1654$ and 0.1655 , and two corresponding members of the family of corotating vortices, $\alpha_0 = 0.087$ and 0.039 , whose conserved properties (circulation, angular momentum,

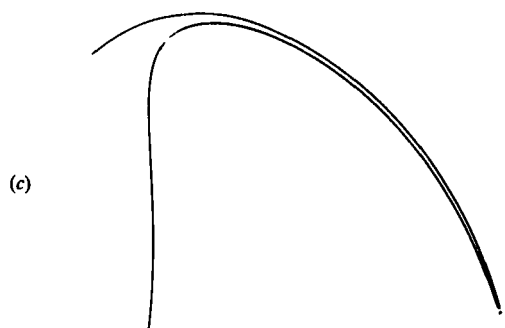
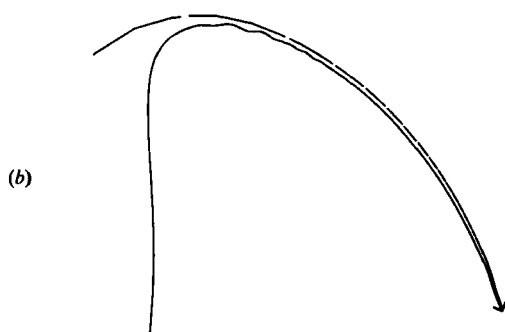
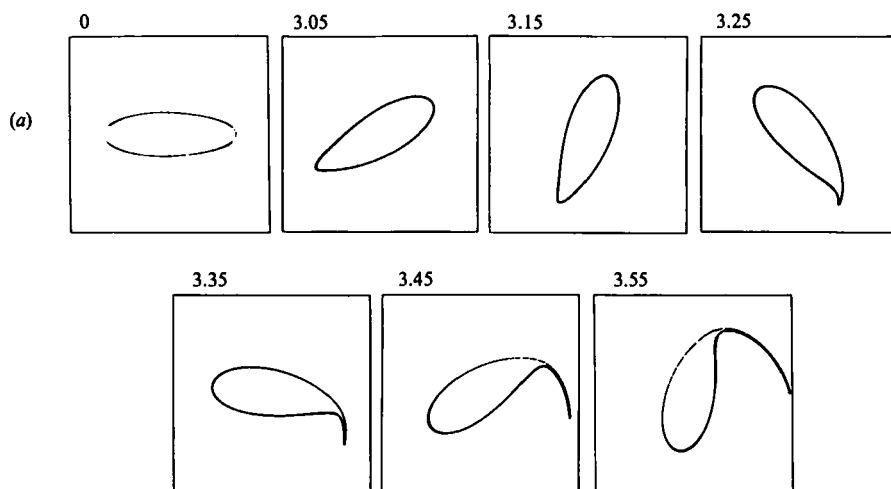


FIGURE 13. (a) 3:1 marginally stable ellipse with a superimposed marginal disturbance ($m = 3$). The first three rotations of the vortex are not shown, but the initial condition is displayed in the first frame. (b) Enlarged view of the last frame in (a) showing numerical instability. (c) As in (b) but with higher resolution (16 Gaussian points instead of 4).

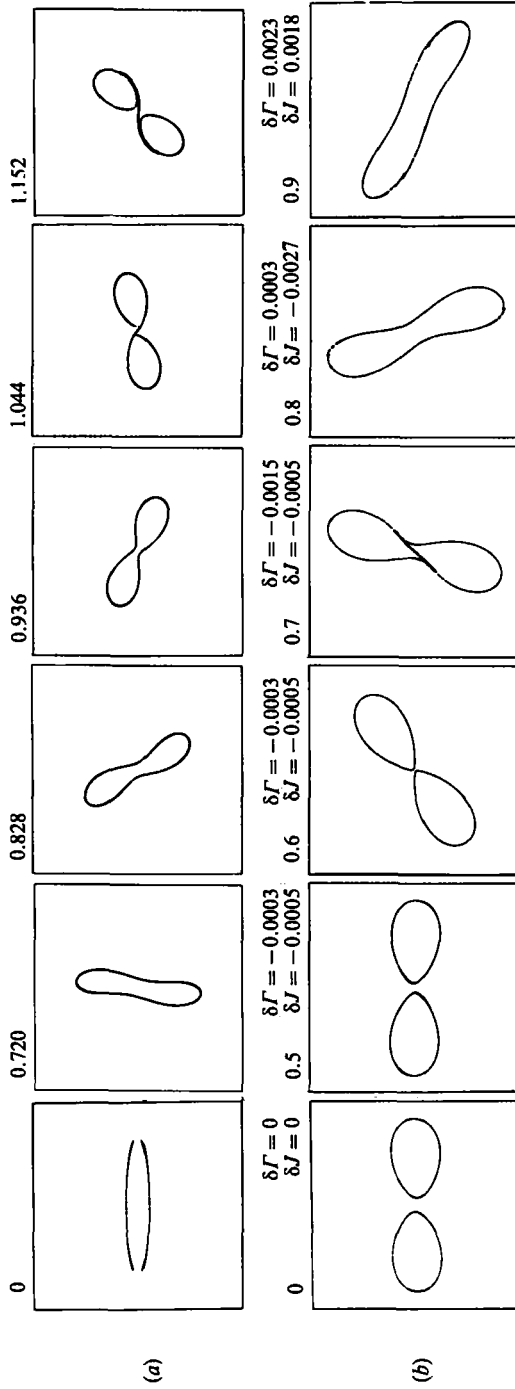


FIGURE 14. (a) 6:1 ellipse transition to two vortices. (b) Converse two-vortex transition to an ellipse. The time is measured relative to the period of rotation of the unperturbed vortices.

centroid, energy, total area and vorticity) are identical. We postulated that a transition is possible between these conjugate states. To test this hypothesis, we calculated the evolution of a $b/a = 0.1655$ ellipse initially perturbed with a hybrid $m = 2$ disturbance: instead of using $\beta = \pm \frac{1}{4}\pi$ for the phase, we used $\beta = -5^\circ, 0$ and 5° . Since the three cases evolved similarly, we show only the case for $\beta = 0$. Figure 14(a) shows the ellipse dividing into two vortices that are *very* close to the $a_0 = 0.087$ steadily corotating configuration. Conversely, using a basic state consisting of two corotating vortices plus a linearly unstable eigenmode (as discussed in the next section), figure 14(b) displays the formation of a $b/a = 0.1655$ ellipse. Contour ‘surgery’ was performed at $t = 0.7$ in order to continue the calculation – the error in doing this is indicated in the relative changes in circulation and angular momentum, of about 0.3%. Soon after, the imprecise surgery caused the development of small cusps and the calculation had to be discontinued, but we do see the initial stages of an ellipse (compare by looking backwards through figure 14a).

It is rather surprising that one slightly perturbed unstable equilibrium can evolve into another unstable equilibrium, given the infinite number of possible evolutionary paths. We conjecture that many evolutionary paths are bundled together owing to the low numbers of unstable linear eigenmodes associated with the two equilibria. For the ellipse, a single even-fold symmetric eigenmode is unstable whereas two corotating vortices are unstable to a single symmetric instability.

The example just presented points to the great practical value of using energetic constraints to understand transitions between different vortex configurations. We propose that the gross evolution of interacting uniform vortices (of the same uniform value of the vorticity) can be predicted by considering (i) the distribution’s location on the energy diagram (figure 1) relative to the energy curves of neighbouring equilibrium distributions, and (ii) the symmetry of the distribution in relation to the symmetries of neighbouring (equilibrium) distributions. The ellipse–two-vortex transition occurs so cleanly because of both the proximity of the two equilibria on the energy diagram (see figure 15), and the common 2-fold symmetry of the ellipse, the two vortices and the imposed disturbance. In contrast, figures 12(b–d) show how symmetry differences between the disturbance and the basic state radically alter predictions based purely upon energetic similarity. We shall return to this proposal in the conclusions after we discuss the results for two, three and four corotating vortices in the next section.

To conclude, we have found that the ellipse is (nonlinearly) stable only if the basic-state ellipse is linearly stable. This agrees with the recent analytical results of Tang (1984). Almost all disturbances to a linearly unstable (or marginal) ellipse have been found to be unstable, the exception being that even-fold symmetry perturbations vacillate when the basic state is only linearly unstable to $m = 3$. When the ellipse is linearly unstable to some $m > 3$, neutral disturbances (with $m \neq 2$) first develop into thin strands of vorticity, followed by the excitation and rapid nonlinear growth of the linearly unstable eigenmodes (e.g. figure 12d).

6. Corotating vortex evolution

Finally, we consider the nonlinear morphology of the equilibria whose form and linear stability were determined in D. For practical reasons, we limit our attention to two, three and four vortices. Each calculation below begins with a slightly perturbed equilibrium of corotating vortices (see table 4). The perturbations consist of eigenfunctions of the linear stability analysis multiplied by a small number ϵ ; the

N	a_0	l	m	Basic-state type	Disturbance type	Nonlinear stability
2	0.10	1	1, 2	Stable	Neutral	Stable
	0.10	2	1, 2	Stable	Neutral	Stable
	0.085	1	2	Stable	Neutral	Stable
	0.08	1	1	Unstable	Neutral	Unstable
	0.08 ^{14b}	1	2	Unstable	Stable and unstable	Unstable
	0.08	2	1, 2	Unstable	Neutral	Unstable
	0.075	1	1	Unstable	Neutral	Unstable
	0.075	1	2	Unstable	Stable and unstable	Unstable
	0.075	2	1, 2	Unstable	Neutral	Unstable
0.04	1	2	Unstable	Unstable	Unstable	
3	0.23	1	1, 2, 3	Stable	Neutral	Stable
	0.23	2	1, 2, 3	Stable	Neutral	Stable
	0.23	3	1, 2, 3	Stable	Neutral	Stable
	0.215	1	1, 2, 3	Unstable	Neutral	Stable
	0.215	2	1, 2, 3	Unstable	Neutral	Unstable
	0.215	3	1+2	Unstable	Stable and unstable	Unstable
	0.215	3	3	Unstable	Neutral	Unstable
	0.20	1	1	Unstable	Neutral	Unstable
	0.20	1	2	Unstable	Stable and unstable	Unstable
	0.20	1	3	Unstable	Neutral	Stable
	0.20	2	1, 2, 3	Unstable	Neutral	Unstable
	0.20 ¹⁶	3	1+2	Unstable	Stable and unstable	Unstable
0.20	3	3	Unstable	Neutral	Unstable	
4	0.38	1	1, 2, 3	Stable	Neutral	Stable
	0.38	2	1, 3	Stable	Neutral	Unstable
	0.38	2	2	Stable	Neutral	Stable
	0.38	3	1, 2, 3	Stable	Neutral	Stable
	0.38	4	1, 2, 3	Stable	Neutral	Unstable
	0.37	1	1, 2, 3	Unstable	Neutral	Stable
	0.37	2	1, 3	Unstable	Neutral	Unstable
	0.37	2	2	Unstable	Neutral	Stable
	0.37	3	1+2	Unstable	Stable and unstable	Unstable
	0.37	3	3	Unstable	Neutral	Stable
	0.37	4	1+2	Unstable	Stable and unstable	Unstable
	0.37	4	3	Unstable	Neutral	Unstable
	0.32 ¹⁷	3	1+2	Unstable	Stable and unstable	Unstable
	0.29	1	2	Unstable	Neutral	Stable
	0.28	1	1	Unstable	Neutral	Unstable
	0.28	1	2	Unstable	Stable and unstable	Unstable
	0.28	1	3	Unstable	Neutral	Stable
	0.28	2	1, 2, 3	Unstable	Neutral	Unstable
	0.28	3	1+2	Unstable	Stable and unstable	Unstable
	0.28	3	3	Unstable	Neutral	Unstable
	0.28	4	1+2	Unstable	Stable and unstable	Unstable
0.28	4	3	Unstable	Neutral	Unstable	
0.26	1	2	Unstable	Stable and unstable	Unstable	
0.24	4	1+2+3	Unstable	Stable and unstable	Unstable	
0.22	4	1+1+2	Unstable	Stable and unstable	Unstable	

TABLE 4. Summary of the corotating vortex calculations. N refers to the number of vortices, a_0 describes the shape of the basic state, and l and m refer to the linear eigenmode. $l = 1$ implies that the disturbance is the same on all the vortices (symmetric) while other values of l imply various kinds of asymmetric disturbances. m is similar to the wavenumber m used for the ellipse and the annular vortex. See D for details. The initial perturbation amplitude is $\epsilon = 0.01$ except for a few cases mentioned in the text. Superscripts denote figure numbers

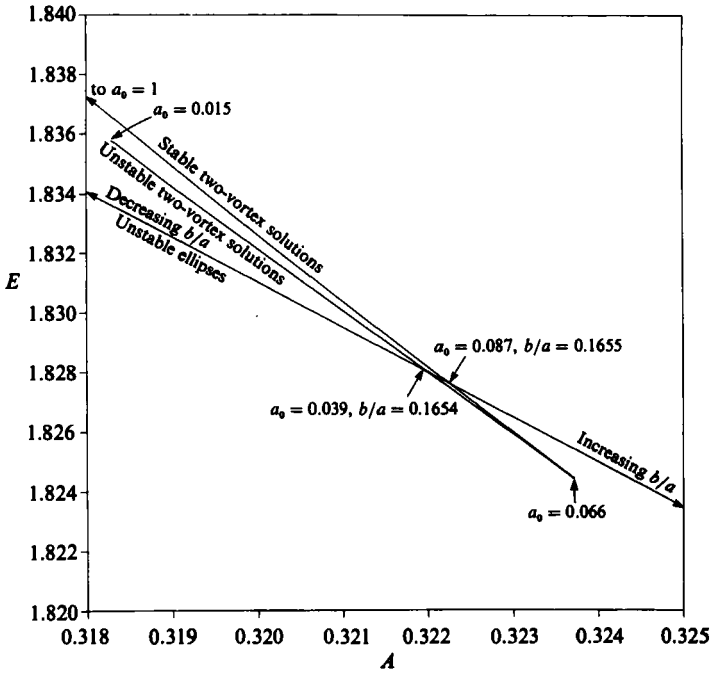


FIGURE 15. Updated energy diagram for the two-vortex family and the ellipses. The two crossing points are where the ellipse is identical, except topologically, with the two vortices.

maximum departure of the boundary from its equilibrium position is ϵ . In table 4, N is the number of vortices, a_0 is the minimum distance, in equilibrium, between the origin and any vortex (unity is the distance to the outermost edge of any vortex), l gives the symmetry of the disturbance, and m indicates the origin of the eigenmode at $a_0 = 1$ (for further details, see D, p. 109, §7.1). The eigenmode on the k th vortex has the form $\text{Re} [w_{lm} \exp(2\pi i(l-1)(k-1)/N)]$ where w_{lm} is a function of position along the equilibrium boundary. An $l = 1$ eigenmode disturbs each vortex identically; m corresponds roughly to azimuthal wavenumber – it is similar to the m used in the previous two sections. To reduce the amount of computation required, only disturbances with non-negative phase speeds are considered. 144 points are used to discretize each vortex's boundary, and $\epsilon = 0.01$ except in a few cases discussed below. All figures give the time relative to the rotation period of the equilibrium configuration.

6.1. Two vortices

We first test the linear stability results by checking the location of the stability boundary. We are implicitly assuming that the nonlinear and linear stability boundaries coincide, just as they have for the ellipse and the annular vortex. The linear analysis yields $a_0 = 0.083$ for the stability boundary. From table 4, the four most fundamental eigenmodes, $(l, m) = (\text{symmetry, azimuthal wavenumber}) = (1, 1), (1, 2), (2, 1)$ and $(2, 2)$ at $a_0 = 0.1$ with $\epsilon = 0.01$ remain small through eight rotation periods, the duration of the calculations. And, as a more stringent test, the $a_0 = 0.085$ configuration perturbed with a $(1, 2)$ eigenmode of amplitude $\epsilon = 0.0015$ resists instability through ten rotation periods. On the other hand, an $a_0 = 0.08$ configuration is unstable to the $(1, 2)$ eigenmode of amplitude $\epsilon = 0.0015$ (the $\epsilon = 0.01$ case is shown in figure 14b). Thus, the worst possible estimate of the stability boundary, is $a_0 = 0.0825 \pm 0.004$.

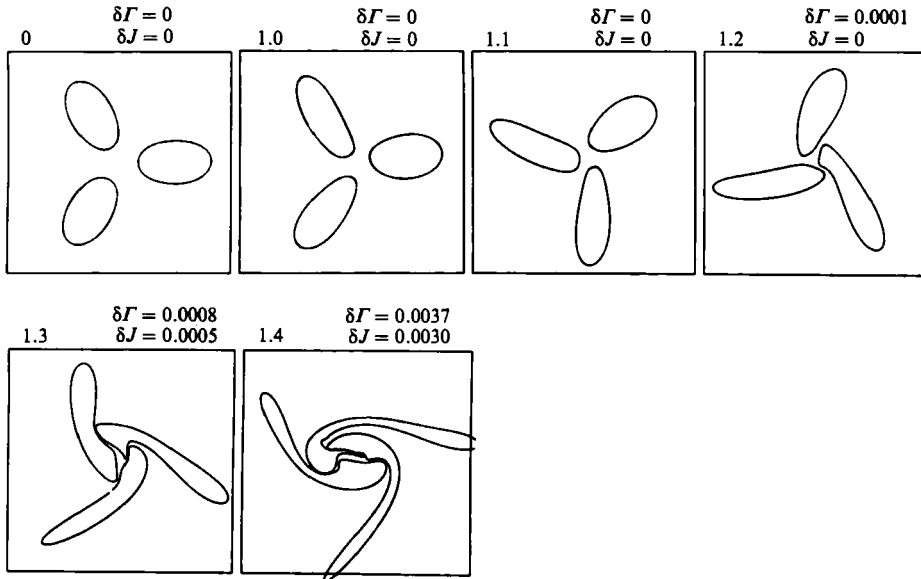


FIGURE 16. The evolution of an asymmetrically perturbed three-vortex state. $\epsilon = 0.02$, $a_0 = 0.2$.

Next, we examine the behaviour of perturbations to a linearly unstable configuration. The $(1, 1)$ eigenmode at $a_0 = 0.08$ with $\epsilon = 0.01$, despite its linear neutrality, excites the $(1, 2)$ mode and also results in vortex ‘merger’, very much like that shown in figure 14(b). The $(1, 1)$ mode for *any* N and a_0 represents a rotation without distortion of the entire configuration to *first order in ϵ* ; second-order effects account for the instability. Disturbances with $l = 2$ also excite the symmetric disturbance and, in all cases, the nonlinear evolution tends towards the formation of a near 6:1 ellipse. Very little formation of small scales occurs during the merger as a consequence of the energetic similarities between the two vortices and the ellipse (see figure 15).

6.2. Three vortices

The linear analysis indicates that three vortices destabilize first to an asymmetric eigenmode $(3, 1+2)$ at $a_0 = 0.223$. The notation ‘ $1+2$ ’ means that the instability derives from the coalescence of the $(3, 1)$ and $(3, 2)$ eigenmodes. At $a_0 = 0.206$, a second instability arises, this time symmetric, as a result of the $(1, 2)$ mode coalescing with its conjugate; for simplicity, we call this combined mode a $(1, 2)$ mode. To test the stability boundaries, we calculated the evolution of the nine most fundamental neutral modes at $a_0 = 0.23$ (see table 4). In all cases, the disturbances remained stable. At $a_0 = 0.215$, all but the $l = 1$ symmetry modes resulted in instability. The neutral asymmetric disturbances ($l = 2$) can apparently generate the unstable eigenmode $(3, 1+2)$. At $a_0 = 0.2$, all disturbances except for $(1, 3)$ result in instability because both symmetric and asymmetric eigenmodes are unstable. The $(1, 3)$ disturbance escapes instability, we suspect, because large- m symmetric modes cannot generate the low- m $(1, 2)$, unstable eigenmode. Finally, our calculations confirm the locations of the marginal stability boundaries found in D.

The unstable disturbances evolve with an appreciable degree of complexity. Figure 16 shows the evolution of the asymmetric eigenmode at $a_0 = 0.2$, with $\epsilon = 0.02$. The three vortices collapse into an annular-like region while ejecting broad streamers of vorticity. These streamers will probably wrap up around the inner annular region,

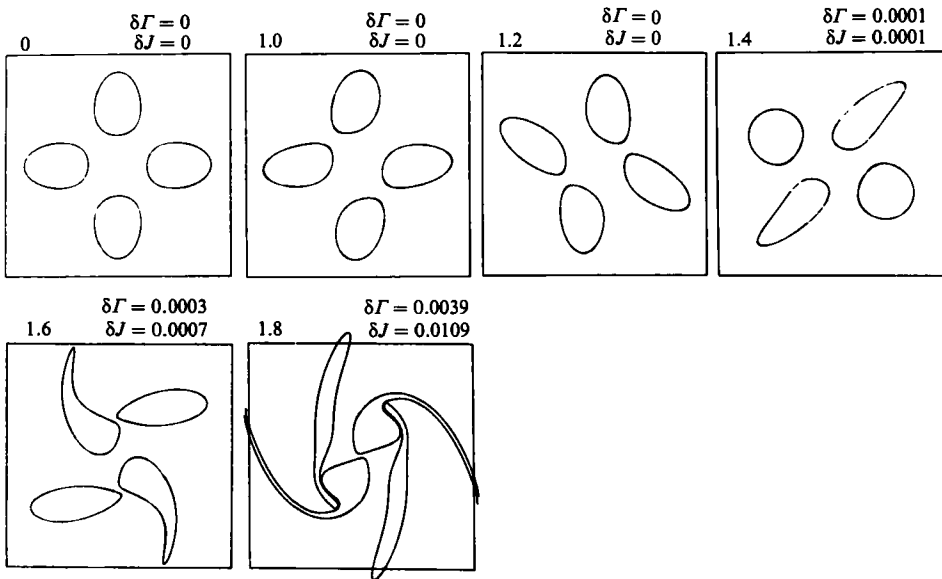


FIGURE 17. The evolution of an antisymmetrically perturbed four-vortex state. $a_0 = 0.32$.

and after a long time, the streamers will be very long and thin but carry a substantial fraction of the total circulation. One cannot be sure that the streamers of vorticity will forever thin and lengthen; since a significant part of the circulation is contained within the streamers, the long-time evolution may depend critically upon the vorticity outside the central vortex. The second instability for three vortices is symmetric and becomes the dominant instability for larger vortices. The collapse of the configuration proceeds, albeit symmetrically, much as in figure 16. Thus for three vortices, the merger process involves the formation of a central vortex and the ejection of substantial amounts of vorticity.

6.3. Four vortices

The linear analysis for four vortices predicts an exceedingly complex stability diagram containing a host of symmetric, antisymmetric and asymmetric instabilities. Only the first few stability boundaries were thoroughly checked, but the nature of the instabilities associated with the other boundaries was determined. Four vortices first destabilize to a $(3, 1+2)$ antisymmetric mode at $a_0 = 0.373$ (the perturbation alternates in sign going from one vortex to the next), then to an asymmetric $(4, 1+2)$ mode at $a_0 = 0.371$, and then to a symmetric $(1, 2)$ mode at $a_0 = 0.283$. The asymmetric mode subsequently disappears at $a_0 = 0.268$, and two additional asymmetric instabilities occur for yet smaller a_0 (larger vortices). Direct calculation shows that the $l = 1$ and 3 disturbances and the $(2, 2)$ disturbance are stable at $a_0 = 0.38$. Most of the asymmetric disturbances are unstable, probably owing to the close proximity of the neutral stability boundary. At $a_0 = 0.37$, the antisymmetric unstable eigenmode $(3, 1+2)$ becomes unstable, but otherwise we find the same stability results as with $a_0 = 0.38$. Just before the symmetric marginal stability boundary ($a_0 = 0.283$), the symmetric $(1, 2)$ disturbance at $a_0 = 0.29$ is stable. But, at $a_0 = 0.28$, the $(1, 2)$ disturbance becomes unstable, in agreement with our linear stability results. For $a_0 = 0.28$, all other disturbances, with the exception of $(1, 3)$, are now unstable. Recall the similar results for three vortices: large- m symmetric

disturbances are stable. In summary, we again find support for the linear analysis of D.

The evolution of four unstable vortices is discussed next. The antisymmetric disturbance is shown in figure 17. First, two sets of two vortices pair and then these two sets pair leaving small and large strands of vorticity dangling from the vortex conglomerate. Four asymmetrically perturbed vortices proceed through successive 'mergers' toward a single large vortex structure surrounded by broad streamers of vorticity. The symmetric instability follows a similar evolution but leaves a large hole of irrotational fluid at the centre (not shown).

To conclude, we find nonlinear stability whenever the configurations are linearly stable. This suggests that there may be a theorem of nonlinear stability like those derived analytically for a circular vortex and an elliptical vortex. Regarding the fate of eigenmode disturbances to linearly unstable equilibria, we find that large- m symmetric neutral disturbances are the only ones that resist instability. The other disturbances eventually cause the collapse of the vortices into a central annular region surrounded by substantial streamers of vorticity except for the clean merger of two vortices into a near 6:1 ellipse. This merger was found to be related to the close proximity of two vortices to the ellipse on the energy diagram. Three and four vortices do not merge cleanly, and we believe that this is a consequence of their energy curves being distant from the energy curves of other equilibria of compatible symmetry. Consider the ' V -states' of Wu *et al.* (1984). These equilibria are N -fold symmetric single vortex configurations with $N = 2$ corresponding to the ellipse. The energy curves for $N = 3$ and 4 are plotted in figure 1, and one can see that transitions are *not* possible between corotating vortices and ' V -states' when $N > 2$. Of course, this does not rule out transitions to more complex equilibria that are yet to be found.

7. Discussion and conclusions

Through direct calculation we have presented the nonlinear morphology of rotating uniform distributions of vorticity. The study covered the evolution and stability of annular, elliptical and corotating vortices. In general, we have found that small disturbances to linearly stable configurations are always stable. For a linearly marginal or unstable configuration, some specific neutral eigenmodes of the correct symmetry can resist instability, depending upon the symmetry of the basic state and upon the symmetry of the unstable eigenmode(s), but most disturbances, and more importantly from the practical standpoint, random disturbances, lead to instability. Thus, one general conclusion is that similar nonlinear stability results exist for a variety of equilibria, leading us to propose that all rotating equilibria are nonlinearly stable in the same parameter range that ensures linear stability.

The character of nonlinear stability has been shown to differ appreciably from that of linear stability. In fact, the only correspondence between them occurs for the initial evolution of linearly unstable eigenmodes. The difference between the two forms of stability are important. First, finite-amplitude linearly neutral or stable disturbances can excite linearly unstable eigenmodes through 'wave-wave' coupling and effect which is second order in disturbance amplitude. Secondly, the initial growth of an instability cannot always be described by linear theory: a thin filament can rapidly grow out of a vortex boundary (such as in figure 12*d*), and the perturbation caused by the filament can subsequently excite unstable modes.

We have observed a strong tendency for unstable configurations to evolve 'close' to other known equilibrium configurations, or near ones that we suspect may be in

equilibrium. This tendency appears to be related to the global properties of the flow (energetics, symmetry) and not, except in detail, to the initial conditions. Given a disturbance of symmetry compatible with that of the basic state, the evolution tends toward other equilibria of compatible symmetry with energetic properties that are most similar. We have presented several examples of this: the ellipse-two-vortex transition (figure 14*a, b*) and the annulus-five-vortex transition (figure 10). On the other hand, if the initial condition is energetically distant from other equilibria of compatible symmetry, a substantial fraction of the circulation is lost to thin strands of vorticity. In numerous examples these thin strands rapidly thinned so as to lose their dynamical significance (but note the formation of the satellite vortex in figure 12*b*). The strands, however, may not always or even often be neglected. Melander, McWilliams & Zabusky (1985) show that the strands cause initially elliptical (non-uniform) vortices to become more circular in time. Recent unpublished calculations by the author show similar results for uniform regions of vorticity. Whether or not significant cascading of small scales occurs during the evolution, the (statistically) final state becomes bound to one particular equilibrium. And, although the fluid may never depart significantly from the equilibrium, small irreversible wave-breaking events can still occur, as was demonstrated in figure 7 of Zabusky (1981) and figure 6 of the present study.

The results of this study may be applicable to various geophysical phenomena. Many observations of tornadoes have shown the breakup of a vortex into several smaller but significantly more intense vortices (Fujita 1970; Agee *et al.* 1977). Often two or three vortices develop, but up to six have been observed. Among the many theoretical attempts to explain this phenomenon, one simple approach has been to assume that multiple vortices result from a largely two-dimensional instability mechanism. In such a case, only the axial vorticity distribution in a cross-section through the vortex is relevant to the determination of stability. Probably the simplest such vorticity distribution that leads to (two-dimensional) linear instabilities favouring low numbers of vortices is the annular vortex. We have determined that these instabilities do indeed evolve into multiple vortices, but, on the other hand, the annular vortex cannot generate the vortex pair so frequently observed in nature. A more viable alternative is offered in Dritschel (1986) in which the *three*-dimensional linear stability of a subclass of vortex flows is considered.

The merger and breakup of vortices occur regularly in geophysical flows. Christiansen & Zabusky (1973), in their study of vortex wakes, used a 'Vortex-in-Cell' model to illustrate the complicated dynamics of interacting vortices. After the wake destabilizes, coherent vortex structures arise which subsequently rip apart and merge. In the stratosphere, where potential vorticity is advected almost conservatively along isentropic surfaces, data (McIntyre & Palmer 1984) show the 'polar-night' vortex, an intense, persistent winter-time vortex, being ripped into two or shedding filaments of vorticity. The vortex appears to rip apart once it has become sufficiently elliptical while the shedding process occurs almost continually when the vortex is dominantly circular, this process apparently developing from small wave-breaking events (McIntyre & Palmer 1984). The understanding of the dynamics of vortex merger and fission would thus aid in the interpretation of many observations, and, as a beginning, the study of simple vorticity distributions may lead to a rough explanation of observed vortex dynamics.

This work has been submitted in partial fulfillment of the requirements for the degree of Ph.D. in the Geophysical Fluid Dynamics Program of Princeton University. The author is grateful to his thesis advisor, Dr R. T. Pierrehumbert, and also Dr I. M. Held for their guidance during the preparation of this manuscript.

Appendix. Calculation of conserved quantities by contour integrals

This Appendix expresses certain area integrals in terms of contour integrals for piecewise-constant vorticity distributions in two dimensions. Consider first the total circulation Γ given by

$$\Gamma = \iint \omega \, dx \, dy = \sum_i \omega_i \iint_{R_i} dx \, dy, \quad (\text{A } 1)$$

where ω_i is the uniform vorticity in region R_i and the sum extends over all such regions. Using Stokes' theorem,

$$\Gamma = \sum_i \frac{1}{2} \tilde{\omega}_i \oint_{C_i} (X_i \, dY_i - Y_i \, dX_i), \quad (\text{A } 2)$$

where $\tilde{\omega}_i$ is the jump in vorticity across the outer boundary, C_i , of R_i (R_i is to the left when traversing C_i in the positive sense: $\tilde{\omega}_i$ is the vorticity just inside C_i minus that just outside), and (X_i, Y_i) is a point on C_i . Consider next the angular momentum (second moment)

$$J = 2 \iint (x^2 + y^2) \omega \, dx \, dy = 2 \sum_i \omega_i \iint_{R_i} (x^2 + y^2) \, dx \, dy. \quad (\text{A } 3)$$

In terms of contour integrals,

$$J = \frac{1}{2} \sum_i \tilde{\omega}_i \oint_{C_i} (X_i^2 + Y_i^2) (X_i \, dY_i - Y_i \, dX_i). \quad (\text{A } 4)$$

The difficult calculation rests with the (excess) energy:

$$T_s = -\frac{1}{2} \iint \omega \psi_s \, dx \, dy, \quad (\text{A } 5)$$

where
$$\psi_s = \frac{1}{2\pi} \iint \log\left(\frac{r}{l}\right) \omega(x', y') \, dx' \, dy', \quad (\text{A } 6)$$

with $l^2 = J/\Gamma$ and $r^2 = (x-x')^2 + (y-y')^2$.

ψ_s can be transformed to

$$4\pi\psi_s = -\Gamma + \sum_i \tilde{\omega}_i \oint_{C_i} \log\left(\frac{r'_i}{l}\right) [(X'_i - x) \, dY'_i - (Y'_i - y) \, dX'_i], \quad (\text{A } 7)$$

where $(r'_i)^2 = (x - X'_i)^2 + (y - Y'_i)^2$. After carrying out extensive algebra, we find that T_s may be expressed in compact form as

$$16\pi T_s = 4\Gamma^2 + \sum_i \sum_j \tilde{\omega}_i \tilde{\omega}_j \oint_{C_i} \oint_{C_j} (r'_{ij})^2 \log\left(\frac{r'_{ij}}{l}\right) dX'_i \cdot dX'_j, \quad (\text{A } 8)$$

where $(r'_{ij})^2 = |X'_j - X'_i|^2$. Computational experience has proven that this expression converges very rapidly with increasing resolution.

REFERENCES

- ABRAMOWITZ, M. & STEGUN, I. A. 1965 *Handbook of Mathematical Functions*. Dover.
- AGEE, E. M., SNOW, J. T., NICKERSON, F. S., CLARE, P. R., CHURCH, C. R. & SCHAAL, L. A. 1977 An observational study of the West Lafayette, Indiana, tornado of 20 March 1976. *Mon. Wea. Rev.* **105**, 893–907.
- BENJAMIN, T. N. & OLVER, P. J. 1982 Hamiltonian structure, symmetries, and conservation laws for water waves. *J. Fluid Mech.* **125**, 137–185.
- CHILDRESS, S. 1984 A vortex-tube model of eddies in the inertial range. *Geophys. Astrophys. Fluid Dyn.* **29**, 29–64.
- CHRISTIANSEN, J. P. 1973 Numerical simulation of hydrodynamics by the method of point vortices. *J. Comp. Phys.* **13**, 363–379.
- CHRISTIANSEN, J. P. & ZABUSKY, N. J. 1973 Instability, coalescence and fission of finite-area vortex structures. *J. Fluid Mech.* **61**, 219–243.
- DEEM, G. S. & ZABUSKY, N. J. 1978a Vortex waves: stationary V -states, interactions, recurrence, and breaking. *Phys. Rev. Lett.*, **40**, 859–862.
- DEEM, G. S. & ZABUSKY, N. J. 1978b Stationary V -states, interactions, recurrence, and breaking. In *Solitons in Action* (ed. K. Longren & A. Scott), pp. 277–293. Academic.
- DRITSCHEL, D. G. 1985 The stability and energetics of corotating uniform vortices. *J. Fluid Mech.* **157**, 95–134.
- DRITSCHEL, D. G. 1986 The stability of vortices in near solid-body rotation. *J. Fluid Mech.* (submitted).
- FUJITA, T. T. 1970 The Lubbock tornadoes: a study in suction spots. *Weatherwise* **23**, 160–173.
- KIRCHHOFF, G. 1876 *Vorlesungen über mathematische Physik*. Leipzig: Mechanik.
- LOVE, A. E. H. 1893 On the stability of certain vortex motions. *Proc. Lond. Math. Soc.* **35**, 18.
- LUNDGREN, T. S. 1982 Strained spiral vortex model for turbulent fine structure. *Phys. Fluids* **25**, 2193–3005.
- MCINTYRE, M. E. & PALMER, T. N. 1984 The ‘surf zone’ in the stratosphere. *J. Atmos. Terr. Phys.* **46**, 825–850.
- MARSDEN, J. E. 1985 Nonlinear stability in fluids and plasmas. Preprint, University of California, Berkeley.
- MEIRON, D. I., SAFFMAN, P. G. & SCHATZMAN, J. C. 1984 The linear two-dimensional stability of inviscid vortex streets of finite-cored vortices. *J. Fluid Mech.* **147**, 187–212.
- MELANDER, M. V., MCWILLIAMS, J. C. & ZABUSKY, N. J. 1986 Circularization and vorticity-gradient intensification of an isolated 2D-vortex. Preprint.
- MICHALKE, A. & TIMME, A. 1967 On the inviscid stability of certain two-dimensional vortex-type flows. *J. Fluid Mech.* **29**, 647–666.
- MOORE, D. W. & GRIFFITH-JONES, R. 1974 The stability of an expanding circular vortex sheet. *Mathematika* **21**, 128.
- OVERMAN, E. A. & ZABUSKY, N. J. 1982 Evolution and merger of isolated vortex structures. *Phys. Fluids* **25**, 1297–1305.
- PIERREHUMBERT, R. T. 1980 A family of steady, translating vortex pairs with distributed vorticity. *J. Fluid Mech.* **99**, 129–144.
- PIERREHUMBERT, R. T. & WIDNALL, S. E. 1981 The structure of organized vortices in a free shear layer. *J. Fluid Mech.* **102**, 301–313.
- SAFFMAN, P. G. & BAKER, G. R. 1979 Vortex interactions. *Ann. Rev. Fluid Mech.* **11**, 95–122.
- SAFFMAN, P. G. & SCHATZMAN, J. C. 1982 Stability of a vortex street of finite vortices. *J. Fluid Mech.* **117**, 171–185.
- SAFFMAN, P. G. & SZETO, R. 1980 Equilibrium shapes of a pair of uniform vortices. *Phys. Fluids* **23**, 2339–2342.
- SNOW, J. T. 1978 On inertial instability as related to the multiple-vortex phenomenon. *J. Atmos. Sci.* **35**, 1660–1667.
- TANG, Y. 1984 Nonlinear stability of vortex patches. Dissertation submitted to the State University of New York at Buffalo.

- WAN, Y. H. & PULVIRENTI, M. 1985 Nonlinear stability of circular vortex patches. *Commun. Math. Phys.* **99**, 435–450.
- WU, H. M., OVERMAN, E. A. & ZABUSKY, N. J. 1984 Steady-state solutions of the Euler equations in two dimensions: rotating and translating V -states with limiting cases. I. Numerical algorithms and results. *J. Comp. Phys.* **53**, 42–71.
- ZABUSKY, N. J. 1981 Recent developments in contour dynamics for the Euler equations in two dimensions. *Ann. N.Y. Acad. Sci.* **373**, 160–170.
- ZABUSKY, N. J., HUGHES, M. H. & ROBERTS, K. V. 1979 Contour dynamics for the Euler equations in two dimensions. *J. Comp. Phys.* **30**, 96–106.